CFSRC COLLOQUIUM

Proceedings of the Cold-Formed Steel Research Consortium Colloquium
20-22 October 2020 (cfsrc.org)

New Proposal for the Shear Strength of Unstiffened Cold-formed Steel Beam Webs

Song Hong Pham[1], Cao Hung Pham[2] and Gregory J Hancock[3]

Abstract

Shear strength of cold-formed steel beam webs is significantly dependent on the end boundary conditions of the shear panels. The North American Specification for the design of cold-formed steel structural members AISI S100-16 Section G2.1 reflects this dependence by recognizing a lower shear capacity for unstiffened shear panels, as low as the elastic shear buckling strength for slender beam webs. This paper presents a series of shear tests on cold-formed steel C-shaped sections with various bolting configurations at the span ends aiming to simulate different degrees of restraint, somewhat close to industry practice. The tests saw a considerable post-buckling shear strength which has not been appreciated by the current Specification. Supported by additional experimental shear strength data from the literature, a new design shear curve is proposed to allow for a higher shear strength of unstiffened panels than the elastic buckling values. Reliability analyses carried out based upon the available test results produce a resistance factor of 0.9 which is consistent with that for bending.

1. Background

1.1 Shear design by the AISI for unstiffened and stiffened panels

Prior to the 2012 edition [1], the North American Specification only permitted shear strength to be computed on the basis of either shear yielding, inelastic buckling or elastic buckling represented by the following design equations:

$$V_n = A_w F_v \quad (1a)$$

For $h/t \le \sqrt{Ek_v/F_y}$

$$F_v = 0.60F_y \quad (1b)$$

For $\sqrt{Ek_v/F_y} < h/t \le 1.51\sqrt{Ek_v/F_y}$

$$F_v = \frac{0.60\sqrt{Ek_vF_y}}{(h/t)} \quad (1c)$$

For $h/t > 1.51\sqrt{Ek_v/F_y}$

$$F_v = \frac{\pi^2 Ek_v}{12(1-\mu^2)(h/t)^2} = 0.904Ek_v/(h/t)^2 \quad (1d)$$

where

V_n = Nominal shear strength,

A_w = Area of web element, $A_w = ht$, (1e)

where

h = Depth of flat portion of web measured along plane of web,

t = Web thickness.

F_v = Nominal shear stress,

E = Modulus of elasticity of steel,

k_v = Shear buckling coefficient calculated in accordance with (1) or (2) as follows:

(1) For unreinforced webs, $k_v = 5.34$

(2) For webs with transverse stiffeners satisfying strength and stiffness requirements stated in Section C3.7:

[1] Doctoral graduate. E-mail: songhong.pham@sydney.edu.au
[2] Senior Lecturer in Structural Engineering, School of Civil Engineering, The University of Sydney, NSW 2006, Australia. E-mail: caohung.pham@sydney.edu.au
[3] Emeritus Professor and Professorial Research Fellow, School of Civil Engineering, The University of Sydney, NSW 2006, Australia. E-mail: gregory.hancock@sydney.edu.au

when a/h ≤ 1.0:

$$k_v = 4.00 + \frac{5.34}{(a/h)^2}$$

when a/h > 1.0:

$$k_v = 5.34 + \frac{4.00}{(a/h)^2}$$

where

a = Shear panel length of unreinforced web element

= Clear distance between transverse stiffeners of reinforced web element

F_y = Design yield stress

μ = Poisson's ratio of steel

= 0.3

The 2012 edition marked a significant change in the design of cold-formed steel structural members in shear with the introduction of shear design in the Direct Strength Method (DSM) in Appendix 1. It is noted that the DSM design had been introduced for compression and bending in 2007. For shear design, while the abovementioned equations (Equations 1a-1d) remained in Section C3.2 of the main body, Sections 1.2.2.2 in the Appendix differentiated beams with and without web stiffeners. When beams are transversely unstiffened (without stiffeners), their shear strength is determined based upon Equations 2a-2c. They are identical to Equation 1 but are reformatted with the inclusion of the section slenderness (λ_v) concept.

For $\lambda_v \le 0.815$

$$V_n = V_y \quad (2a)$$

For $0.815 < \lambda_v \le 1.227$

$$V_n = 0.815\sqrt{V_{cr}V_y} \quad (2b)$$

For $\lambda_v > 1.227$

$$V_n = V_{cr} \quad (2c)$$

where:

$$\lambda_v = \sqrt{\frac{V_y}{V_{cr}}} \quad (2d)$$

V_y = Yield shear force of cross-section,

$$V_y = 0.6A_wF_y \quad (2e)$$

V_{cr} = Elastic shear buckling force of section

These design equations are shown graphically in Figure 1 (solid curve) resulting from fitting thirty-five shear test results conducted by LaBoube and Yu [2]. It is noted that eight other experimental results have been discarded due to non-shear failure modes as discussed in [3]. For transversely stiffened members, the 2012 version of the AISI included the Pham and Hancock [3] findings, the dashed curve in Figure 1, which accounts for shear post-buckling strength of stiffened shear panels having shear span aspect ratios (shear-span/web-depth) not greater than 2.0. Their tests, which are discussed in the following section, demonstrate a considerable shear strength development subsequent to elastic web shear buckling. The extent of the post-buckling strength is represented by the difference between the two curves in Figure 1 which is more significant in the high slenderness range.

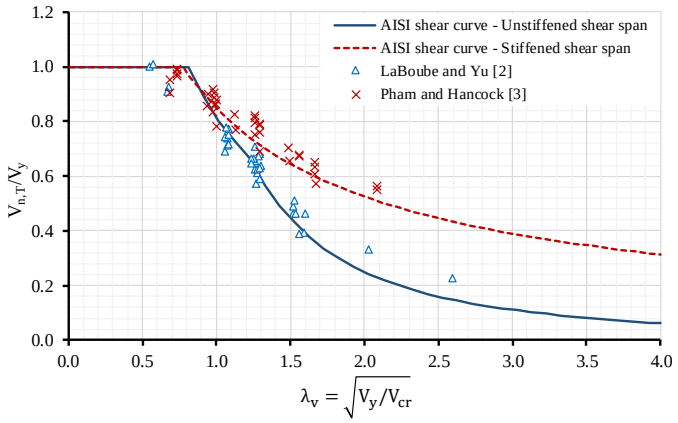

Figure 1: Current design shear curves

The higher tier shear strength curve is expressed by the following design equations in the Direct Strength Method format:

For $\lambda_v \le 0.776$

$$V_n = V_y \quad (3a)$$

For $\lambda_v > 0.776$

$$V_n = \left[1 - 0.15\left(\frac{V_{cr}}{V_y}\right)^{0.4}\right]\left(\frac{V_{cr}}{V_y}\right)^{0.4} V_y \quad (3b)$$

where V_y and V_{cr} have been defined previously.

It is interesting to see that the format of Equations 3a-3b including the power (0.4) and the multiplier (0.15) are identical to those of the DSM equations for compression and flexural members under local buckling. This similarity demonstrates the dominant nature of local shear postbuckling in webs.

1.2 Post buckling shear strength

As mentioned, the Pham and Hancock tests [3] appear to mobilize the full shear post-buckling strength mainly contributed by Tension Field Action (TFA). Despite still being a controversial topic with different opinions as summarized in [4], the discussion of the mechanism and formation of shear post-buckling is out of the scope of this

paper. It is therefore assumed the primary role of the TFA in the development of additional shear strength subsequent to shear buckling.

Table 1 shows the extent of shear strength enhanced by the TFA in the Pham and Hancock shear test series [3] across a wide spectrum of section slenderness (λ_v) as given by Equation 2d sorted in ascending order. In Table 1, $V_{n,T}$ and V_y are the experimental shear strength and shear yield load, respectively; V_{cr} is the elastic shear buckling load determined by the Semi-Analytical Finite Strip method based computer program bfinst8.cpp [5]; V_{pb} is the shear post-buckling strength, computed as $V_{pb} = V_{n,T} - V_{cr}$ and V_{pb} is taken as zero when $V_{n,T}$ is less than V_{cr}.

Table 1: Shear postbuckling in Pham and Hancock tests

Test	Section	Shear Span (mm)	Aspect Ratio	t (mm)	$V_{n,T}$ (kN)	V_y (kN)	V_{cr} (kN)	λ_v	$V_{n,T}/V_y$	V_{pb} (kN)	V_{pb}/V_{cr} (%)
V1	SC15024	150	1.0	2.4	98.0	103	220	0.68	0.95	0.00	0.00
Vw	SC15024	150	1.0	2.4	92.9	103	220	0.68	0.91	0.00	0.00
Vw	C15024	150	1.0	2.4	93.4	96.6	179	0.73	0.97	0.00	0.00
V2	C15024	150	1.0	2.4	96.0	96.7	179	0.74	0.99	0.00	0.00
V1	C15024	150	1.0	2.4	94.2	96.9	179	0.74	0.97	0.00	0.00
V3	C15024	150	1.0	2.4	95.6	96.9	179	0.74	0.99	0.00	0.00
Vw	SC20024	200	1.0	2.4	117	137	155	0.94	0.86	0.00	0.00
V1	SC20024	200	1.0	2.4	124	138	155	0.94	0.9	0.00	0.00
Vw	C15019	150	1.0	1.9	70.9	84.9	88.4	0.98	0.84	0.00	0.00
V3	C15019	150	1.0	1.9	77.9	85.0	88.3	0.98	0.92	0.00	0.00
V1	C15019	150	1.0	1.9	76.8	85.0	88.2	0.98	0.9	0.00	0.00
V2	C15019	150	1.0	1.9	75.7	85.1	88.2	0.98	0.89	0.00	0.00
V3	C20024	200	1.0	2.4	113	131	133	0.99	0.86	0.00	0.00
V2	C20024	200	1.0	2.4	114	131	133	1.00	0.87	0.00	0.00
V1	C20024	200	1.0	2.4	115	132	132	1.00	0.88	0.00	0.00
Vw	C20024	200	1.0	2.4	103	132	132	1.00	0.78	0.00	0.00
V1	SC15015	150	1.0	1.5	55.6	67.1	53.3	1.12	0.83	2.26	4.24
Vw	SC15015	150	1.0	1.5	51.9	67.6	52.9	1.13	0.77	0.00	0.00
V2	C15015	150	1.0	1.5	56.1	68.3	43.2	1.26	0.82	12.9	29.8
Vw	C15015	150	1.0	1.5	51.3	68.3	43.2	1.26	0.75	8.09	18.7
V1	C15015	150	1.0	1.5	55.4	68.4	43.1	1.26	0.81	12.3	28.5
V3	C15015	150	1.0	1.5	54.5	68.4	43.1	1.26	0.8	11.3	26.3
V3	C20019	200	1.0	1.9	83.4	109	65.9	1.29	0.76	17.4	26.4
Vw	C20019	200	1.0	1.9	75.8	110	65.9	1.29	0.69	9.89	15.0
V1	C20019	200	1.0	1.9	86.5	110	65.8	1.29	0.79	20.7	31.4
V2	C20019	200	1.0	1.9	86.1	110	65.8	1.29	0.79	20.2	30.7
V1	SC15012	150	1.0	1.2	42.1	59.9	27	1.49	0.7	15.1	56.0
Vw	SC15012	150	1.0	1.2	39.3	60.1	26.9	1.49	0.66	12.4	46.0
V1	SC20015	200	1.0	1.5	62.1	91.4	37.4	1.56	0.68	24.6	65.8
Vw	SC20015	200	1.0	1.5	61.7	91.4	37.4	1.56	0.68	24.2	64.8
V2	C20015	200	1.0	1.5	53.9	88.5	31.9	1.67	0.61	22.0	69.1
V3	C20015	200	1.0	1.5	57.8	88.6	31.9	1.67	0.65	25.9	81.4
V1	C20015	200	1.0	1.5	56.1	88.6	31.8	1.67	0.63	24.3	76.3
Vw	C20015	200	1.0	1.5	50.8	88.6	31.8	1.67	0.57	19.0	59.7
V1	SC20012	200	1.0	1.2	46.5	82.5	19	2.09	0.56	27.5	145
Vw	SC20012	200	1.0	1.2	45.6	82.6	18.9	2.09	0.55	26.6	141

Note: 'W' means 'Without Straps'

It can be seen that post-buckling strength starts occurring at a λ_v value of 1.12, relatively close to the inelastic buckling limits shown in Equation 2. In addition, a higher degree of postbuckling strength occurs for the slenderer sections, as high as 145%. In fact, the LaBoube and Yu tests [2] showed a certain extent of TFA, up to 51.5%, in the elastic buckling range although it has not been accounted for in Equation 1.

1.3 Influence of end boundary conditions on shear strength

Figure 2 and 3 show the experimental set-up and typical shear failure modes observed in the LaBoube and Yu tests (Figure 2) and in the Pham and Hancock tests (Figure 3).

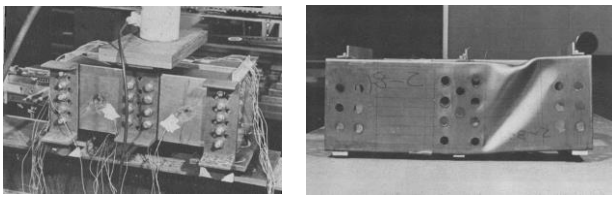

Figure 2: Shear test by LaBoube and Yu [2]

Figure 3: Shear test by Pham and Hancock [3]

In general, these two test setups are very similar in terms of the toe-to-toe channel configuration, mid-span point load application and bolting connections. However, it appears that the LaBoube and Yu tests included variability in the end boundary conditions where five rows of bolts are observed in the left image, but only three are seen in the right image. In this image, the shear failure band only occurred in the right-hand side shear span whereas the left was still intact indicating perhaps a high degree of imperfection on the right side. Slightly differently, Pham and Hancock employed consistently more rows of bolts spanning across the full depth of the webs (four rows for 150mm deep and five rows for 200mm deep C-sections). These observations are not considered to be conclusive but they are essential to explain the significant discrepancy between the normalized ultimate shear strengths at a specific section slenderness of the two test series as seen in Figure 1.

To study the influence of end span bolting configurations on the development of shear post-buckling strength, CH Pham et al. [6] conducted shear tests with a similar setup as mentioned previously but with one or two rows of bolts

removed in a manner that disadvantaged the development of the TFA as seen in Figure 4.

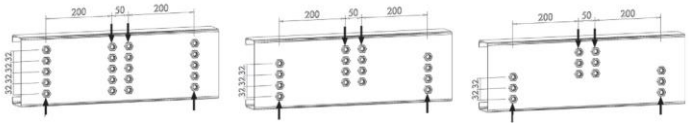

Figure 4: Bolt patterns studied by CH Pham et al. [6]

Not surprisingly, the removal of bolts altered the modes of failure which involved a noticeable lateral distortion of the flanges at support locations (Figure 5b). This penalized the ultimate shear strength by 33% and 53% on average for tests with one bolt and two bolts removed, respectively. Despite restraint being provided against this lateral deformation by fixing the strap to the support plate (see Figure 5c), shear strength reduction is still significant compared with the fully bolted tests with 9% and 34% decrease.

(a) (b) (c)

Figure 5: Failure modes of tests with one and two rows off

These tests have demonstrated the critical role of end boundary conditions on the development of the TFA. Variation of bolting configurations influences the extent of restraints along the web depth, thus altering the formation of buckling mode shapes and it might induce a complex mode of failure at significantly lower ultimate loads. The following sections present additional experiments with other bolting patterns representing a various degree of end shear span restraints, somewhat close to practical connections being used in industry.

2. Shear tests with partial end restraints

2.1 Test setup and test procedure

The experimental program was performed using a dual actuator test rig [7] which has been demonstrated to be successful in conducting shear tests with shear span aspect ratios up to 2.0 [8–10]. A detailed description of the test configuration can be found in the abovementioned references, only a brief description is provided herein. Figure 6 shows a schematic diagram of the main features of the test setup.

The beam was loaded by two actuators via two 20 mm loading plate assemblies bolted to the beam web. Each MTS actuator has a capacity of 253 kN in compression and 162 kN in tension, and a stroke of 508 mm. They are controlled simultaneously by an MTS FlexTest® Controller. These actuators are able to move independently with different rates, adding the flexibility in controlling the loading process. In Figure 6, only one channel is shown for clarity. The actual test comprised of two channels bolted back to back to the two sides of the loading plates.

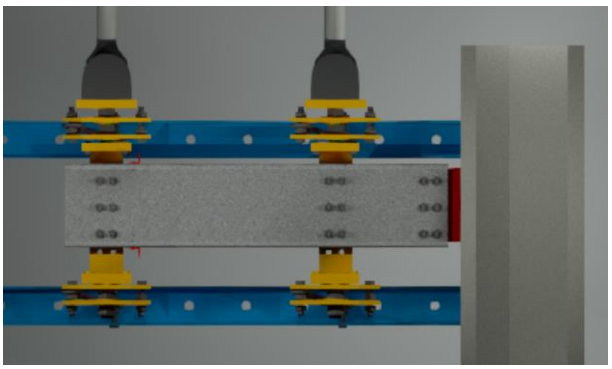

Figure 6: Diagram of the test setup

Figure 7 shows an actual cold-formed steel beam under loading. An additional 92mm channel section stiffener was screwed to the span adjacent to the shear span of interest to avoid possible premature combined bending and shear failure. A default movement rate of 0.5 mm/min was used for both actuators at the beginning of the tests.

Figure 7: Test specimen under loading

2.2 Instrumentation

During the tests, six linear variable displacement transducers (LVDTs) were used to track the vertical displacements along the specimens' length. The locations of the instruments are shown in Figure 7. Vishay Model 5100B scanners and the Vishay System 5000 StrainSmart® software were used to record the measured data.

2.3 Experimental schedule

Two commercially common cross-sectional types in Australia including 200mm deep, 1.5mm thick plain C-section and 200mm deep, 1.2mm thick SupaCee® sections were used. The SupaCee® is different from the plain-C by having return lip and four small longitudinal stiffeners on its web. Six different bolting configurations at the ends of shear spans as illustrated in Figure 8 were studied. Based upon the standard five rows of bolts over the full web depth which has been used successfully to mobilize full TFA [3], five different configurations were adopted by removing up to three rows of bolts. Unlike the bolt patterns studied by Pham CH et al. [6] where the bolts along the diagonal TFA line were removed, in this test program, bolts are symmetrically reduced at both ends about the mid-web depth.

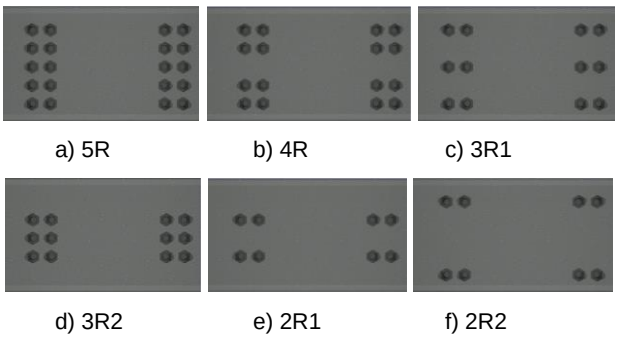

a) 5R b) 4R c) 3R1

d) 3R2 e) 2R1 f) 2R2

Figure 8: End-span bolt configurations

2.4 Experimental Results

Table 2: Experimental results

Test Designation	Shear Span (mm)	Aspect Ratio	t (mm)	f_y (MPa)	$V_{n,T}$ (kN)	V_{cr} (kN)	V_y (kN)	λ_v	$V_{n,T}/V_y$
SC20012-5R-1-WS	200	1.0	1.2	601.2	30.7	21.6	82.2	1.95	0.37
SC20012-5R-2-WS	200	1.0	1.2	601.2	33.5	21.6	82.2	1.95	0.41
SC20012-5R-1-NS	200	1.0	1.2	601.2	34.9	21.6	82.2	1.95	0.42
SC20012-5R-2-NS	200	1.0	1.2	601.2	34.7	21.6	82.2	1.95	0.42
SC20012-5R-3-NS	200	1.0	1.2	601.2	33.8	21.6	82.2	1.95	0.41
SC20012-4R-1-NS	200	1.0	1.2	601.2	31.2	21.6	82.2	1.95	0.38
SC20012-4R-2-NS	200	1.0	1.2	601.2	29.7	21.6	82.2	1.95	0.36
SC20012-3R1-1-NS	200	1.0	1.2	601.2	33.8	21.6	82.2	1.95	0.41
SC20012-3R1-2-NS	200	1.0	1.2	601.2	34.3	21.6	82.2	1.95	0.42
SC20012-3R2-1-NS	200	1.0	1.2	601.2	14.7	21.6	82.2	1.95	0.18
SC20012-3R2-2-NS	200	1.0	1.2	601.2	14.7	21.6	82.2	1.95	0.18
SC20012-3R2-3-NS	200	1.0	1.2	601.2	16.0	21.6	82.2	1.95	0.19
C20015-5R-1-WS	200	1.0	1.5	554.8	45.2	32.0	94.9	1.72	0.48
C20015-5R-2-WS	200	1.0	1.5	554.8	48.8	32.0	94.9	1.72	0.51
C20015-5R-1-NS	200	1.0	1.5	554.8	40.7	32.0	94.9	1.72	0.43
C20015-5R-2-NS	200	1.0	1.5	554.8	40.8	32.0	94.9	1.72	0.43
C20015-5R-3-NS	200	1.0	1.5	554.8	41.4	32.0	94.9	1.72	0.44
C20015-3R1-1-NS	200	1.0	1.5	554.8	44.6	32.0	94.9	1.72	0.47
C20015-3R2-1-NS	200	1.0	1.5	554.8	25.0	32.0	94.9	1.72	0.26
C20015-3R2-2-NS	200	1.0	1.5	554.8	28.4	32.0	94.9	1.72	0.30
C20015-2R1-1-NS	200	1.0	1.5	554.8	27.2	32.0	94.9	1.72	0.29
C20015-2R2-1-NS	200	1.0	1.5	554.8	34.5	32.0	94.9	1.72	0.36

Table 2 summarizes the experimental results including material yield stress, ultimate shear force ($V_{n,T}$), shear bucking force (V_{cr}) determined using the finite strip analysis based programme bfinst8.cpp [5], shear yield force (V_y) determined by Equation 2e, section slenderness (λ_v) and the ratio of experimental shear strength ($V_{n,T}$) to shear yield strength (V_y). It is noted that V_{cr} is determined by the software which is based on the assumption that the two ends of the shear span are fully simply supported, i.e. the variation of the end restraints as a result of altering bolt configurations is not accounted for. The test designation, SC20012-5R-1-WS for example, includes the following information:

- Section types: 'SC' for SupCee (alternatively 'C' for plain-C)
- Section depth: 200mm
- Thickness: 1.2mm
- Bolt configuration: 5R as per Figure 8
- Order of the test in the same test configuration: 1st
- Equal angle straps on top and bottom flanges: 'WS' stands for with straps (alternatively 'NS' stands for no straps)

As can be seen from the table, with five rows of bolts spanning over the full depth of the webs and with the straps on the top and bottom flanges, the ultimate shear strengths obtained in this test series are considerably smaller than the strengths obtained by Pham CH and Hancock [3], averaging 31% for the SupaCee and 16% for the plain-C sections. Experiments with five rows of bolts but without straps also show shear strength reductions of 24% and 19% compared with the Pham CH and Hancock tests [3] for the SupaCee and the plain-C sections, respectively. Noticeably, folding patterns occurred at just above the top row of bolts which induced significant lateral deformation of the segment above the folding lines as seen in Figure 9, similar to the observation in the Pham et al. tests [6]. This deformation appears to be involved in the diagonal shear band which potentially lowers the ultimate shear strength. In practice, such deformations might not occur as the flanges are screwed to sheathings and are braced by adjacent joints.

Figure 9: The formation of lateral deflection above the top bolts

It is also evident from Table 2 that reducing the middle row (configuration 4R) or two intermediate rows (3R1) does not noticeably decrease the ultimate shear strength compared to the 5R cases mentioned previously. Diagonal shear

bands developed in both the SupaCee and the plain-Cee sections as shown in Figure 10a. However, a certain degree of out-of-plane deformation causing section distortion was observed. In contrast, other cases including with three rows of bolts centred at mid-web (3R2) or with two rows of bolts only, significant out-of-plane distortion of the flanges or webs occurred which fundamentally changed the failure modes to a more complex combination of failure mechanisms. Ultimate shear strengths, therefore, were lowered considerably.

a) 3R1 b) 3R2

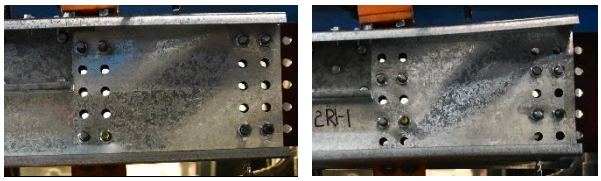

c) 2R1 d) 2R2

Figure 10: Failure modes of tests with various bolt patterns

Figure 11 shows the experimental shear strengths in relation to current shear strength design curves including the higher tier curve with TFA (Equation 3) and the curve without TFA (Equation 2).

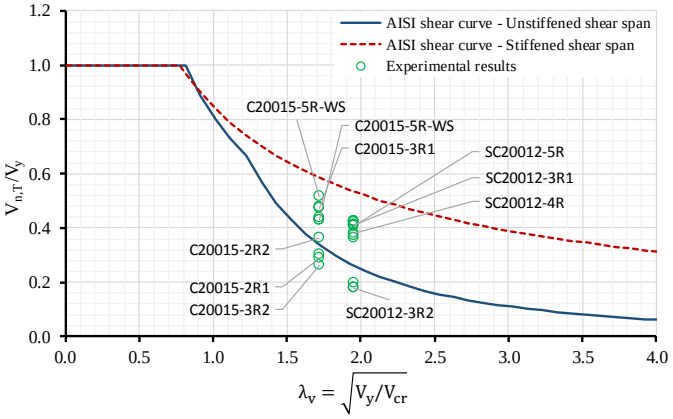

Figure 11: Test results plotted against design shear curves

The values of the section slenderness depicted on the horizontal axis and the experimental shear strength to shear yield force ratio depicted on the vertical axis are included in Table 2. In general, tests with inadequate end shear span restraints (3R2; 2R1; 2R2) are located below the elastic buckling shear curve. In fact, it might be unreasonable to compare these tests with the shear curve as they experienced complex buckling and failure modes rather than close-to-shear failure. The points corresponding to the experiments which were mainly governed by shear are located in-between the two shear curves. They demonstrated that a certain extent of shear postbuckling has been developed but that the end restraints are not sufficient to support the full development.

3. Proposal for shear strength of unstiffened shear panels accounting for post-buckling

Figure 12 shows all of the test results in the literature where TFA is considered as not fully mobilised. They include the LaBoube and Yu tests [2] which have been used to calibrate the current AISI shear curve for unstiffened shear panels; three tests by Keerthan and Mahendran [11] in which no straps were used and it appears that two rows of bolts were employed at the ends of the shear spans to fix the channel webs to the supports via a web plate; four tests by Pham et al. [6] with one row of bolt removed along the diagonal tension field as mentioned previously (other bolt removal patterns are not included as the tests experienced combined complex failure modes rather than shear failure); and the tests described in this paper in Table 2 excluding the 2R1, 2R2, 3R2 tests. The full set of data used for Figure 12 is given in Appendix A. The tests with the bolting configurations 3R2, 2R1 and 2R2, referred to as inadequate end restraint in this paper, are excluded from the data as they are believed to be not qualified for a shear strength study. In Figure 12, the three curves include the two current shear design for unstiffened and stiffened shear panels as per the AISI S100-16, and the dotted curve which is an extension of the curve segment corresponding to the inelastic buckling.

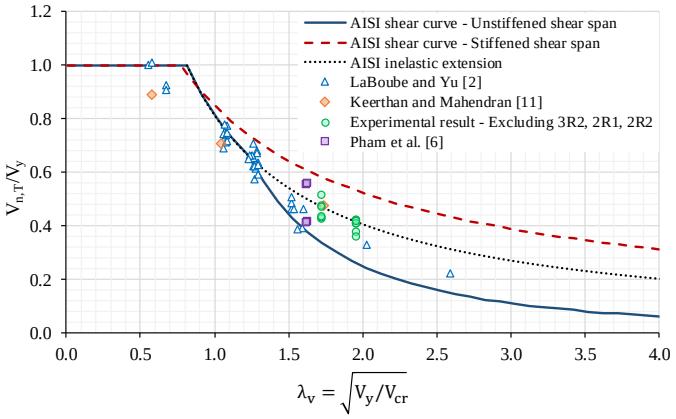

Figure 12: Available unstiffened shear test results plotted against design shear curves

The data demonstrates a slightly different trend compared with the two current shear curves. For relatively low section slenderness (less than 1.0), it shows that current design rules are unconservative, whereas in the elastic range, the

tests are distributed in-between the two curves and closer to the lower one, indicating that a certain degree of TFA has been mobilized. The inelastic extension (dotted curve) is somewhat capable of capturing this enhanced shear strength, but it is slightly too optimistic, and is not able to reflect the lower capacity in the low slenderness range. It is worth noting that an inelastic extension has been adopted recently in the Specification for Structural Steel Buildings AISC 360-16 [12] to replace the yielding-inelastic buckling-elastic buckling shear curve. However, this adoption appears to be unsuitable to cold-formed steel sections.

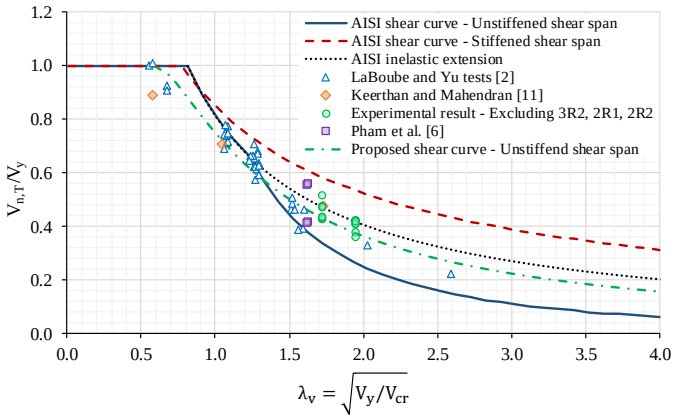

Figure 13: Proposed shear curve

A new shear curve, the dashed-dotted in Figure 13, and expressed in Equation 4 below, has been proposed to reflect better the variation of the test data and to address the un-conservatism of the inelastic extension curve.

For $\lambda_v \le 0.587$

$$V_n = V_y \tag{4a}$$

For $\lambda_v > 0.587$

$$V_n = \left[1 - 0.25\left(\frac{V_{cr}}{V_y}\right)^{0.65}\right]\left(\frac{V_{cr}}{V_y}\right)^{0.65} V_y \tag{4b}$$

where V_y and V_{cr} have been defined previously.

It leverages the simplicity of the DSM design format while providing better shear strength predictions in the low slenderness range as well as accounting for shear-post buckling in the high slender range.

4. Calibrations and design curve selections

The resistance factor (ϕ) associated with the shear strength determined by the proposal as per Equations 4a and 4b is computed using the AISI S100-16 [13] Equation K2.1.1-2 as follows:

$$\phi = C_\phi (M_m F_m P_m)\, e^{-\beta_o \sqrt{V_M^2 + V_F^2 + C_P V_P^2 + V_Q^2}} \tag{5}$$

where

- M_m is the mean value of material factor with its associated coefficient of variation of V_M;
- F_m is the mean value of fabrication factor with its associated coefficient of variation of V_F;
- P_m is the mean value of professional factor taken as 1.03 as shown in Appendix A;
- V_P is the coefficient of variation of the test results, computed as the ratio of the standard deviation of the test-to-predicted ratios to P_m. These two values are shown in Appendix A, thus V_P takes a value of 0.09;
- V_Q is the coefficient of variation of the load effect, taken as 0.21 for Load and Resistance Factor Design (LRFD) as specified by the AISI S100-16;
- C_P is the correction factor for sample size, $C_P = \left(1 + \frac{1}{n}\right) m/(m-2)$, where n=57 is the number of tests, m=n-1=56 is the degree of freedom; as a result, C_P=1.055;

For LRFD, the calibration coefficient (C_ϕ) is taken as *1.52*, and the target reliability index (β_o) is *2.5* for structural members as per the AISI S100-16. The values of M_m, V_M, F_m and V_F are taken as *1.100*; *0.100*; *1.000* and *0.050* in accordance with the AISI S100-16. With the target reliability index of *2.5*, a resistance factor (ϕ) of *0.911* is obtained. In fact, this reduction factor is smaller than the factor of 0.95 which is being specified by the AISI S100-16. However, this reduction can be well justified by the better shear strength prediction accuracy in the low slenderness range, and the considerable shear strength enhancement in the high slenderness range.

5. Conclusion

The current shear strength design equations in the AISI S100-16 Specification are reviewed with reference to the original experiments used to derive these design guidelines. It is evident that post-buckling shear strengths exist even though the shear spans are not fully stiffened. A series of tests have been conducted with various stiffening in the ends of the shear spans to support this assertion. All available shear experiments in the literature which are considered as having unstiffened shear spans have been plotted against the current shear design curves. A new variation of the shear strength has been revealed from the experimental database, and a new DSM-format-based equation has been proposed to capture this new trend. The calibration of the test data shows that a shear strength reduction factor of 0.9 is recommended.

Appendix A: Data used to calibrate proposed curve

Sources	Test designation	V_T (kN)	V_y (kN)	V_{cr} (kN)	λ_v	V_T/V_y	$V_{n,proposed}$	$P_m = V_T/V_{n,proposed}$
Yu and LaBoube [2]	S-1-1	19.1	19.1	62.9	0.55	1.00	19.1	1.00
	S-1-2	19.2	18.9	57.3	0.58	1.01	18.9	1.01
	S-2-1	17.2	23.3	20.2	1.07	0.74	16.4	1.05
	S-2-2	17.4	23.4	21.0	1.06	0.74	16.7	1.04
	S-3-1	17.8	28.0	16.6	1.30	0.64	16.4	1.09
	S-3-2	18.8	27.5	16.6	1.29	0.68	16.2	1.16
	S-8-1	16.7	23.3	20.2	1.08	0.71	16.4	1.02
	S-8-2	16.9	23.5	20.0	1.08	0.72	16.4	1.03
	S-9-1	16.9	27.5	16.8	1.28	0.61	16.4	1.03
	S-9-2	18.7	27.8	16.8	1.29	0.67	16.4	1.14
	S-9-4	17.1	27.4	17.3	1.26	0.62	16.6	1.03
	S-9-5	15.9	27.7	17.2	1.27	0.57	16.6	0.96
	S-9-6	18.4	28.0	17.6	1.26	0.66	16.9	1.09
	S-9-7	12.9	27.9	12.2	1.52	0.46	13.9	0.93
	S-9-8	13.6	27.9	12.1	1.52	0.49	13.8	0.98
	S-10-4	25.4	27.3	60.2	0.67	0.93	26.6	0.95
	S-10-5	24.9	27.4	60.5	0.67	0.91	26.7	0.93
	S-11-1	25.6	41.0	25.3	1.27	0.62	24.5	1.04
	S-11-2	28.8	40.6	25.5	1.26	0.71	24.5	1.18
	S-11-3	27.3	41.3	26.2	1.25	0.66	25.0	1.09
	S-12-1	20.0	51.2	20.2	1.59	0.39	24.1	0.83
	S-12-2	23.9	51.5	20.1	1.60	0.46	24.2	0.99
	S-12-3	20.6	53.0	21.7	1.56	0.39	25.5	0.81
	S-17-1	27.4	41.2	27.0	1.24	0.66	25.4	1.08
	S-17-2	26.7	41.2	27.1	1.23	0.65	25.4	1.05
	S-18-1	26.8	52.5	22.6	1.52	0.51	26.0	1.03
	S-18-2	24.4	52.6	22.4	1.53	0.46	25.9	0.94
	S-19-3	18.4	55.6	13.5	2.03	0.33	20.0	0.92
	S-20-3	15.5	68.7	10.2	2.60	0.22	18.5	0.84
	MS-2-1	17.5	23.4	19.8	1.09	0.75	16.3	1.08
	MS-2-2	17.8	22.9	19.4	1.09	0.77	16.0	1.11
	MS-3-1	17.5	27.9	16.7	1.29	0.63	16.4	1.07
	MS-3-2	16.5	27.9	16.7	1.29	0.59	16.4	1.00
	MS-8-1	18.0	23.2	20.3	1.07	0.78	16.4	1.10
	MS-8-2	16.2	23.5	20.9	1.06	0.69	16.7	0.97
Keerthan and Mahendran [11]	200x75x15x1.50	45.5	95.8	31.9	1.73	0.47	41.1	1.11
	120x50x18x1.50	39.6	56.1	51.7	1.04	0.71	40.6	0.98
	120x50x18x1.95	33.4	37.6	114.1	0.57	0.89	37.6	0.89
Experimental Results	SC20012-5R-1-NS	34.9	82.2	21.6	1.95	0.42	30.9	1.13
	SC20012-5R-2-NS	34.7	82.2	21.6	1.95	0.42	30.9	1.12
	SC20012-5R-3-NS	33.8	82.2	21.6	1.95	0.41	30.9	1.10
	SC20012-3R1-1	33.8	82.2	21.6	1.95	0.41	30.9	1.09
	SC20012-3R1-2	34.3	82.2	21.6	1.95	0.42	30.9	1.11
	SC20012-4R-1	31.2	82.2	21.6	1.95	0.38	30.9	1.01
	SC20012-4R-2	29.7	82.2	21.6	1.95	0.36	30.9	0.96
	SC20012-5R-1-WS	30.7	82.2	21.6	1.95	0.37	30.9	0.99
	CSC20012-5R-2-WS	33.5	82.2	21.6	1.95	0.41	30.9	1.09
	C20015-3R1-1	44.6	94.9	32.0	1.72	0.47	41.0	1.09
	C20015-5R-1-NS	40.7	94.9	32.0	1.72	0.43	41.0	0.99
	C20015-5R-2-NS	40.8	94.9	32.0	1.72	0.43	41.0	0.99
	C20015-5R-3-NS	41.4	94.9	32.0	1.72	0.44	41.0	1.01
	C20015-5R-1-WS	45.2	94.9	32.0	1.72	0.48	41.0	1.10
	C20015-5R-2-WS	48.8	94.9	32.0	1.72	0.51	41.0	1.19
Pham et. al [6]	C20015-1Rw-1	36.4	86.5	32.7	1.63	0.42	39.9	0.91
	C20015-1Rw-2	35.7	86.1	32.8	1.62	0.41	39.9	0.90
	C20015-1Rr-1	47.7	86.0	32.9	1.62	0.56	39.9	1.20
	C20015-1Rr-2	48.7	86.4	32.7	1.63	0.56	39.9	1.22
							Mean	1.03
							SD	0.09
							CoV (%)	8.92

References

[1] AISI, North American specification for the design of cold-formed steel structural members, in: S100-12th ed., Washington, D.C, U.S.A, 2012.

[2] R.A. LaBoube, W.W. Yu, Structural behavior of beam webs subjected primarily to shear, Missouri, USA, 1978.

[3] C.H. Pham, G.J. Hancock, Direct Strength Design of Cold-Formed C-Sections for Shear and Combined Actions, J. Struct. Eng. ASCE. 138 (2012) 759–768. doi:10.1061/(ASCE)ST.1943-541X.0000510.

[4] S.H. Pham, Design of Cold-Formed Steel Beams with Holes and Transverse Stiffeners in Shear, (2019).

[5] G.J. Hancock, C.H. Pham, Shear buckling of channel sections with simply supported ends using the semi-analytical finite strip method, Thin-Walled Struct. 71 (2013) 72–80. doi:10.1016/j.tws.2013.05.004.

[6] C.H. Pham, D. Zelenkin, G.J. Hancock, Effect of flange restraints on shear Tension Field Action in cold-formed C-sections, J. Constr. Steel Res. 129 (2017) 42–53. doi:10.1016/j.jcsr.2016.10.014.

[7] S.H. Pham, C.H. Pham, C.A. Rogers, G.J. Hancock, Experimental validation of the Direct Strength Method for shear spans with high aspect ratios, J. Constr. Steel Res. 157 (2019) 143–150. doi:10.1016/J.JCSR.2019.02.018.

[8] D.K. Pham, C.H. Pham, S.H. Pham, G.J. Hancock, Experimental investigation of high strength cold-formed channel sections in shear with rectangular and slotted web openings, J. Constr. Steel Res. 165 (2020) 105889. doi:https://doi.org/10.1016/j.jcsr.2019.105889.

[9] S.H. Pham, C.H. Pham, G.J. Hancock, Transverse Stiffener Requirements for Shear Postbuckling of Cold-Formed Steel Channels, J. Struct. Eng. 146 (2020) 4020148. doi:10.1061/(ASCE)ST.1943-541X.0002706.

[10] S.H. Pham, C.H. Pham, C.A. Rogers, G.J. Hancock, Shear Strength Experiments and Design of Cold-Formed Steel Channels with Web Holes, J. Struct. Eng. (United States). 146 (2020) 1–14. doi:10.1061/(ASCE)ST.1943-541X.0002464.

[11] P. Keerthan, M. Mahendran, Experimental investigation and design of lipped channel beams in shear, Thin-Walled Struct. 86 (2015) 174–184. doi:10.1016/j.tws.2014.08.024.

[12] AISC, Specification for Structural Steel Buildings, American Institute of Steel Construction, Chicago, Illinois 60601-1802, U.S.A, 2016.

[13] AISI, North American Specification for the Design of Cold-Formed Steel Structural Members, S100-16th ed., Washington, D.C, U.S.A, 2016.